Mining of Mineral Deposits
Volume 20 (2026), Issue 1, 52-58

MMD JOURNAL / MINING.IN.UA

https://doi.org/10.33271/mining20.01.052

Study on the influence of the law of mine thermal environment on the temperature variation of airflow

Zhiyuan Shen [1*], Yimeng Li [1], Qizheng Wang [1]

[1] *School of Civil Engineering, Shenyang Jianzhu University, Liaoning, China*

**Corresponding author: e-mail szy0207@szju.edu.cn*

Abstract

Purpose. The purpose of this paper is to explore the influence of factors such as humidity and wind speed on the change in air flow temperature in a mine thermal environment.

Methods. The mine heat and humidity exchange experiment is combined with numerical simulation. Using ANSYS Fluent, the influence of airflow humidity on the temperature field is simulated and analyzed at different temperatures and wind speeds. A similar experiment was conducted in an experimental mine and measured under different temperature and wind speed conditions. Change in heat exchange between the air inlet and the surrounding rock of the roadway with different humidity.

Findings. Numerical simulation and experimental results show that as the relative humidity in the airflow increases, the rate of rise in airflow temperature increases gradually. The maximum is 0.038°C/m. Higher wind speed shortens the time for heat exchange, reducing the rate of temperature increase. An empirical model was developed to describe the relationships among wind speed, temperature, humidity, and the rate of temperature rise.

Originality. This paper incorporates humidity as a key factor and establishes an empirical model for airflow temperature change in humid mine conditions.

Practical implications. The findings provide a scientific basis for predicting and controlling airflow temperature in high-temperature mines, improving thermal comfort and safety for underground workers and guiding mine ventilation system design and thermal hazard mitigation.

Keywords: *mine; thermal environment; ANASYS Fluent; numerical simulation; temperature change; heat exchange*

1. Introduction

With the continuous increase in global energy demand, the depth and scale of underground mining are expanding, and the thermal environment in mines is becoming increasingly severe [1]. Mine heat damage is mainly caused by underground temperature rise, heat release from mechanical equipment, and the mine ventilation system [2]-[4]. The high-temperature environment not only affects miners' work efficiency and health but can also lead to the failure of mine equipment and even increase the risk of accidents, such as mine fires. Therefore, it is important to study the changing laws of the mine thermal environment [5]-[7].

Guo et al. [8] proposed a wind flow temperature prediction model for the tunneling face that accounts for the coupling effects of multiple heat sources and conducted numerical simulations and verifications, providing a theoretical basis for the design of wind flow temperature control in high-temperature environments in coal mines. Reference [9] compared the heat exchange characteristics between the air flow and the surrounding rock under two ventilation methods in deep mines through numerical simulation and found that the "parallel ventilation" had a higher heat exchange efficiency. Li et al. [10] systematically analyzed the influence of multiple parameters on heat exchange performance, providing an important basis for the design of mine ventilation systems. Ghoreishi et al. [11] proposed a new performance analysis model for a mine tail air waste heat recovery system that considered a coupled heat exchanger. The new model can increase thermal energy recovery efficiency by approximately 20%, significantly reduce the airflow temperature at the working face, and this has been verified through case studies. Bao et al. [12] systematically identified the familiar sources of waste heat in mines and the technologies for their recovery and utilization. Li et al. [13] developed a model for coupling water transfer between air flow and heat transfer in the surrounding rock. They analyzed the influence of the latent heat of evaporation on the prediction of air-flow temperature. Reference [14] explored the control effect of collaborative geothermal resource development on heat hazards in deep mines through numerical simulation. Wang et al. [15] conducted a numerical simulation of the roadway in a high-temperature coal seam working face. They studied the influence of ventilation parameters on the airflow temperature field and the cooling effect. Li et al. [16] analyzed the influence of a movable insulation layer on heat transfer during high-temperature tunnel excavation through numerical simu-

Received: 11 September 2025. Accepted: 23 February 2026. Available online: 30 March 2026

© 2026. Z. Shen, Y. Li, Q. Wang

Mining of Mineral Deposits. ISSN 2415-3443 (Online) | ISSN 2415-3435 (Print)

This is an Open Access article distributed under the terms of the Creative Commons Attribution License (http://creativecommons.org/licenses/by/4.0/), which permits unrestricted reuse, distribution, and reproduction in any medium, provided the original work is properly cited.

lation. The results show that installing an insulation layer can effectively reduce the tunnel's internal temperature and improve construction safety. Wang et al. [17] studied the distribution characteristics of the airflow temperature field in a roadway through on-site measurements and CFD simulations. Jia et al. [18] proposed a dynamic ventilation control model that couples airflow and heat flow. Zhao et al. [19] revealed the laws and critical conditions of the airflow temperature field in ultra-deep shafts, which vary with the conveying height. Kang et al. [20] compared airflow temperature evolution and effective ventilation distance under different cooling strategies in high-temperature tunnels. The results show that the surrounding rock pre-cooling scheme can extend the effective ventilation distance by 30% and is suitable for a continuous tunneling environment in deep coal mines. Che et al. [21] systematically studied the depth-dependent thermal permeability of the surrounding rock of deeply buried high-temperature tunnels through theoretical analysis and on-site and laboratory temperature measurement experiments.

Scholars have made significant contributions and achieved excellent results. However, previous studies have mainly simulated the thermal environment of dry roadways, rather than that of a humid environment. At the same time, an influence model for my airflow temperature change has not yet been established. Therefore, ANSYS Fluent software is used in this study to simulate airflow temperature changes for different humidity and airflow speeds through roadways at different temperatures, and similar simulations are carried out. An empirical model of wind speed, temperature, and humidity influencing factors and the rate of air temperature rise is established to provide a powerful reference for the treatment of mine thermal damage.

2. Numerical simulation

2.1. Basic theory

The dynamic control equation used in the simulation of the mine thermal environment is shown in Equations (1) ~ (5) [22]-[24].

2.1. Continuity equation

Based on the conservation of mass, the continuity equation is derived from the theory that the fluid mass remains constant during normal motion.

$$\frac{\partial \rho}{\partial t}+\frac{\partial(\rho u)}{\partial x}+\frac{\partial(\rho v)}{\partial y}+\frac{\partial(\rho w)}{\partial z}=0 \quad , \tag{1}$$

where:

ρ – density, kg/m^3;

t – time, s;

u, v, w – the velocity vector referring to the component of the velocity on the x, y, and z axes, respectively.

2.2. Equation of motion

The momentum conservation equation is a natural law that must be observed in the actual fluid flow. Momentum conservation considers the fluid to be composed of one microelement, and the ratio of momentum to time of the microelement is the rate of change in momentum, which is the sum of the forces acting on the microelement. According to this calculation method, the momentum conservation law is derived as follows:

$$\frac{\partial(\rho u)}{\partial t}+div(\rho u U)=-\frac{\partial p}{\partial x}+\frac{\partial \tau_{xx}}{\partial x}+\frac{\partial \tau_{yx}}{\partial y}+\frac{\partial \tau_{zx}}{\partial z}+F_x; \tag{2}$$

$$\frac{\partial(\rho v)}{\partial t}+div(\rho v U)=-\frac{\partial p}{\partial y}+\frac{\partial \tau_{xy}}{\partial x}+\frac{\partial \tau_{yy}}{\partial y}+\frac{\partial \tau_{zy}}{\partial z}+F_y; \tag{3}$$

$$\frac{\partial(\rho w)}{\partial t}+div(\rho w U)=-\frac{\partial p}{\partial z}+\frac{\partial \tau_{xz}}{\partial x}+\frac{\partial \tau_{yz}}{\partial y}+\frac{\partial \tau_{zz}}{\partial z}+F_z, \tag{4}$$

where:

p – the pressure on the fluid element, Pa;

τ_{xx}, τ_{yx}, τ_{zx} – the component of the micromolecular viscous resistance on the x, y, and z axes, s;

F_x, F_y, F_z – are the forces acting on the element, N.

2.3. Energy equation

This paper mainly studies the thermal environment of mines, and uses the energy conservation equation with the temperature field as the primary research object, ignoring the mutual conversion between internal energy and heat energy of air flow in the process of fluid flow, and obtains the relevant energy conservation equation:

$$\frac{\partial T}{\partial t}+\frac{\partial(uT)}{\partial x}+\frac{\partial(vT)}{\partial y}+\frac{\partial(wT)}{\partial z}= =\frac{\partial}{\partial x}\left(\frac{k}{c_P\rho}\frac{\partial T}{\partial x}\right)+\frac{\partial}{\partial y}\left(\frac{k}{c_P\rho}\frac{\partial T}{\partial y}\right)+\frac{\partial}{\partial z}\left(\frac{k}{c_P\rho}\frac{\partial T}{\partial z}\right)+S_T, \tag{5}$$

where:

c_P – the specific heat capacity of the fluid, kg/(kg·°C);

T – the temperature,°C;

K – the thermal conductivity;

S_T – is the viscous dissipation term, J.

2.2. Model building

2.2.1. Simulation hypothesis

In practice, applying numerical simulation software to model heat transfer between the surrounding rock and air flow in an experimental mine is highly complex and influenced by many factors. It is almost impossible to build a numerical model based entirely on the actual conditions in the tunnel. Therefore, to simplify the calculation, the following simplifying assumptions are made [25]-[27]:

1. Through the measurement of the initial data, this study assumes that the temperature of the four wall surfaces of the rock is constant, and the temperature of each surface of the rock is evenly distributed.

2. Assuming that the gas in the roadway is ideal and incompressible, the viscous resistance of the air flow is ignored, and the dissipative heat caused by the work of the air itself and the self-compression heat of the air are simplified.

3. Ignoring the heat dissipation of other heat sources and assuming that the air flow is stable, turbulence will not occur because the roadway is too long.

2.2.2. Geometric model and meshing

To ensure the simulation's authenticity, a geometric model is established from measured data from the experimental mine. Owing to the instability of the wind speed in the experimental mine, detailed wind speed measurements are carried out at the selected experimental points, and the section with relatively stable wind flow is selected. The tunnel is 30 m long, 2.5 m high, and 3 m wide, as shown in Figure 1a, to establish a geometric model.

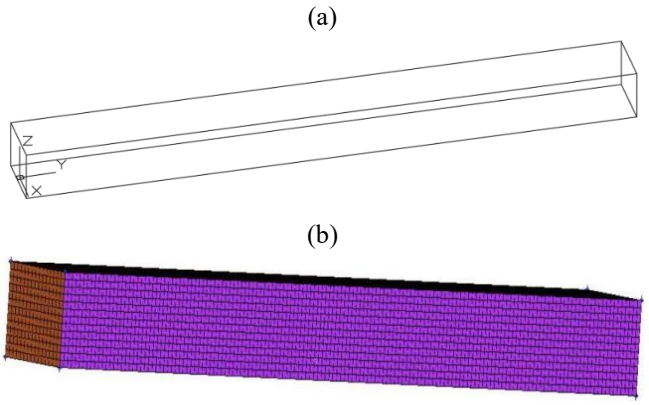

Figure 1. Geometry and mesh of the numerical model: (a) geometric representation of the experimental tunnel; (b) computational grid generated in ICEM

The ICEM software with good mesh quality is selected, a structural division is performed to generate the geometric model's mesh, and a tetrahedral mesh is generated. The model's mesh step is 0.1 m; a total of 312500 mesh elements are used, and the mesh quality is concentrated between 0.95 and 1. The geometric mesh division is shown in Figure 1b.

2.2.3. Geometric model and meshing

2.2.3.1. Analysis of humidity on temperature field variation at different wind speeds

The section is set as the test point for the actual measurement data in the experiment. To make the observation clear, the tunnel section where the airflow is fully preheated is selected. Figure 2 shows the cloud map of *the* $Y = 24$ m cross section at 60, 70 and 80% relative humidity under different wind speeds, at the same time and temperature conditions.

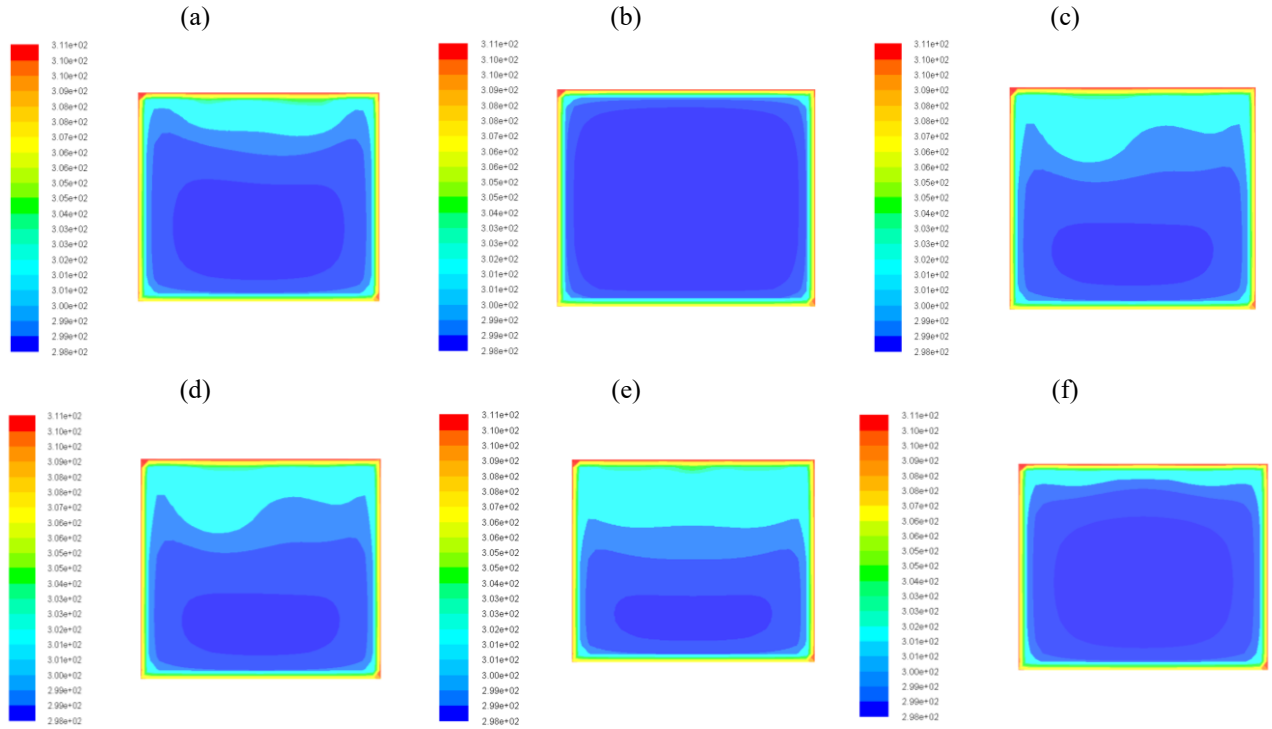

Figure 2. Cloud diagram of Y = 24 m cross section at T = 35°C and different wind speeds and humidity: (a) V = 0.5 m/s, RH = 60%; (b) V = 2m/s, RH = 60%; (c) V = 0.5 m/s, RH = 70%; (d) V = 2m/s, RH = 70%; (e) V = 0.5 m/s, RH = 80%; (f) V = 2m/s, RH = 80%

It can be seen from Figure 2 that the air flow temperature in the tunnel is low inside and high outside, and a large number of blue or blue-green low-temperature areas are concentrated in the lower part of the tunnel's center. This is mainly because the temperature of the roadway wall is much higher than that of the airflow, and the airflow near the wall can conduct sufficient convective heat transfer and absorb radiation heat, resulting in a faster temperature rise and forming a high-temperature circle around the wall. Under the action of gravity, it is evident that a low-temperature area sinks in the roadway, and as humidity decreases, the blue low-temperature air gradually increases. Changes in humidity clearly influence the temperature field. When the humidity is higher, the blue low-temperature region is smaller. When relative humidity is constant, an increase in wind speed increases the evaporation rate of water, and the rate of rise in air temperature slows. When the radiation model is applied, increased relative humidity results in a higher concentration of water vapor in the air. As the concentration of water molecules increases, the wind's capacity to absorb radiation increases. Consequently, water molecules absorb more radiant heat, causing the wind flow to warm faster.

2.2.3.2. Analysis of humidity on temperature field variation at different temperatures

Figure 3 shows the cloud map of the cross section at $Y = 24$ m with relative humidity of 60, 70 and 80% at different temperatures, at the same time, and at the same wind speed.

As shown in Figure 3, the influence of humidity on the temperature field is relatively similar. When the temperature in the roadway is 30°C, it is relatively close to the wind speed temperature, resulting in a large blue area of low temperature. As temperature increases, relative humidity increases, which has a positive effect on radiation heat dissipation. According to the heat transfer formula, the higher the temperature, the higher the internal energy of the gas molecules and the more intense the molecular heat transfer.

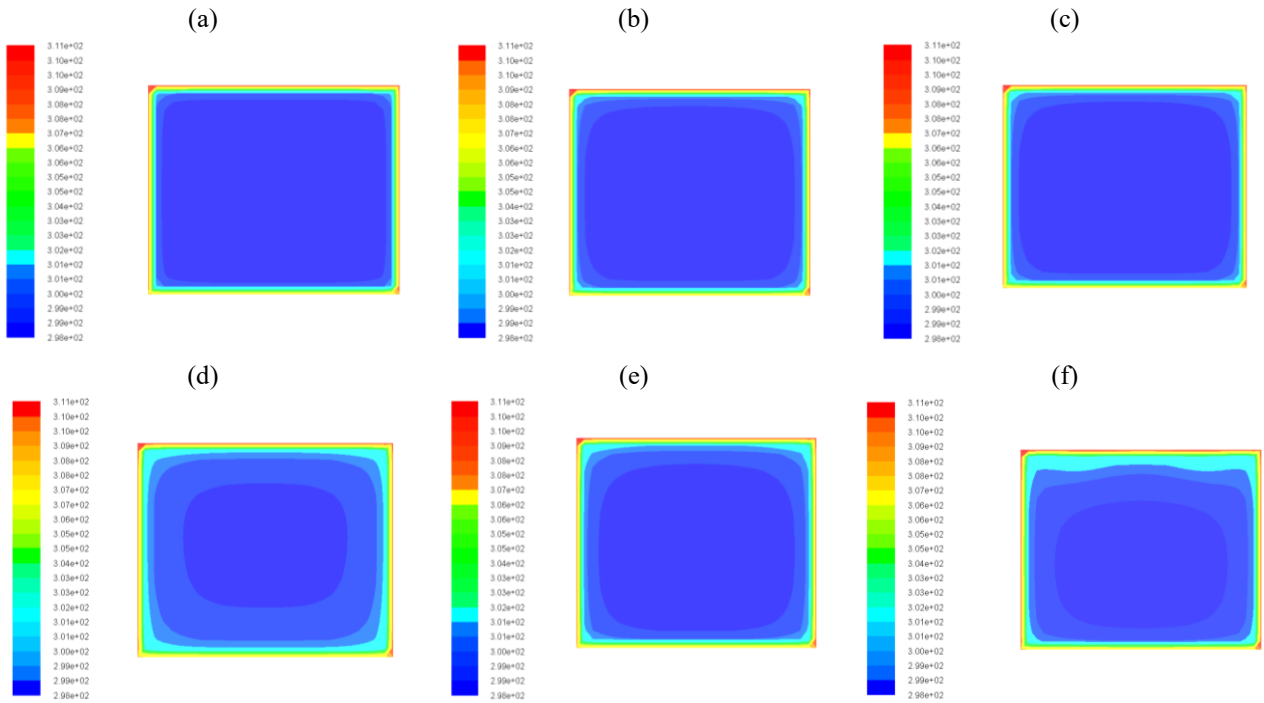

Figure 3. Cloud diagram of Y = 24 m cross section at V = 2m/s and different temperature and humidity: (a) T = 30°C; RH = 60%; (b) T = 35°C; RH = 60%; (c) T = 30°C; RH = 70%; (d) T = 35°C; RH = 70%; (e) T = 30°C; RH = 80%; (f) T = 35°C; RH = 80%

When heat exchange occurs, the degree of heat exchange in the low-temperature air flow is greater, and the speed decay becomes too rapid. However, due to the significant temperature difference in the roadway, the effect of humidity on water evaporation and heat absorption is minimized. It is verified from the side that the influence of temperature on the mine thermal environment is greater than that of humidity.

Using the numerical simulation software Fluent to model heat and moisture transfer between the surrounding rock and wind flow yields some preliminary results. As the humidity increased, the temperature increased more rapidly. To further discuss the accuracy of the simulation law, similar experiments are carried out in Section 3.

3. Simulated tunnel experiment

In the case of different wall temperatures, different inlet air speeds, and different tunnel supply air temperatures, the tunnel supply air parameters, such as inlet air humidity, were varied. The surrounding rock of the experimental roadway exchanged heat and humidity with the airflow under different air-supply parameters. Changes in the temperature and humidity fields under different working conditions were obtained. The measurement observation points are shown in Figure 4.

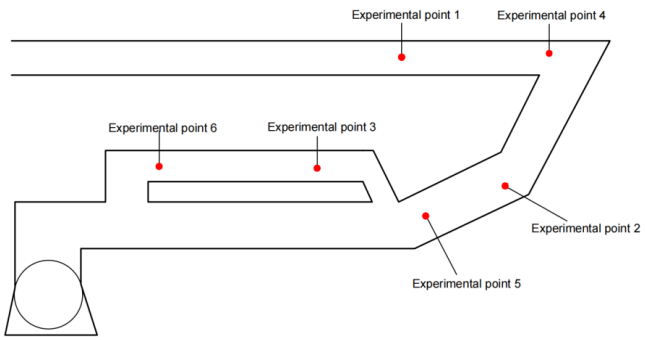

Figure 4. Experimental site layout of the experimental roadway

3.1. Analysis of mine air flow temperature change

During the experiment, the roof temperature in the tunnel is 38°C, the two sides are at 35°C, the bottom is at 30°C, and the initial air inlet temperature is approximately 25.9°C. The experiment starts 30 m before the experimental point; measurements are taken every 6m, and the average of the three measurements is taken. The data graph was drawn using Origin software. Figure 5 shows the trend in airflow temperature at 50, 60, 70 and 80% relative humidity, 30 and 35°C inside the tunnel, and 0.5, 1 and 2 m/s wind speed.

As shown in Figure 5, with increasing humidity, the air temperature rise rate gradually increases, reaching a maximum of 0.038°C/m. This is mainly because increased humidity reduces the rate of water evaporation. At the same time, the concentration of water molecules in the air also enhances the rock's capacity for heat radiation exchange. The inlet air flows continuously through the roadway, and the roadway wall raises the air's temperature. The temperature gradually increases, reducing the temperature difference between the airflow and the wall. According to the heat transfer formula, as the temperature difference between the air flow and the surrounding rock decreases, the heat absorbed by the air flow from the wall also decreases, the temperature rise rate of the air flow decreases, and the temperature rise becomes slow. Moreover, with the increase in the wind speed, the heat exchange time between the air flow and the surrounding rock becomes shorter, which affects the intensity of convective heat transfer and leads to the slow rise of the air flow temperature, making the temperature difference between the outlet temperature and the inlet temperature smaller and smaller.

To explore the relationship between the wind speed and initial temperature in the tunnel, and the exponential function coefficient. With A in $y = Ae^{Bx}$ as the first coefficient and B as the second coefficient, multiple fitting is performed using the cftool toolbox in MATLAB software.

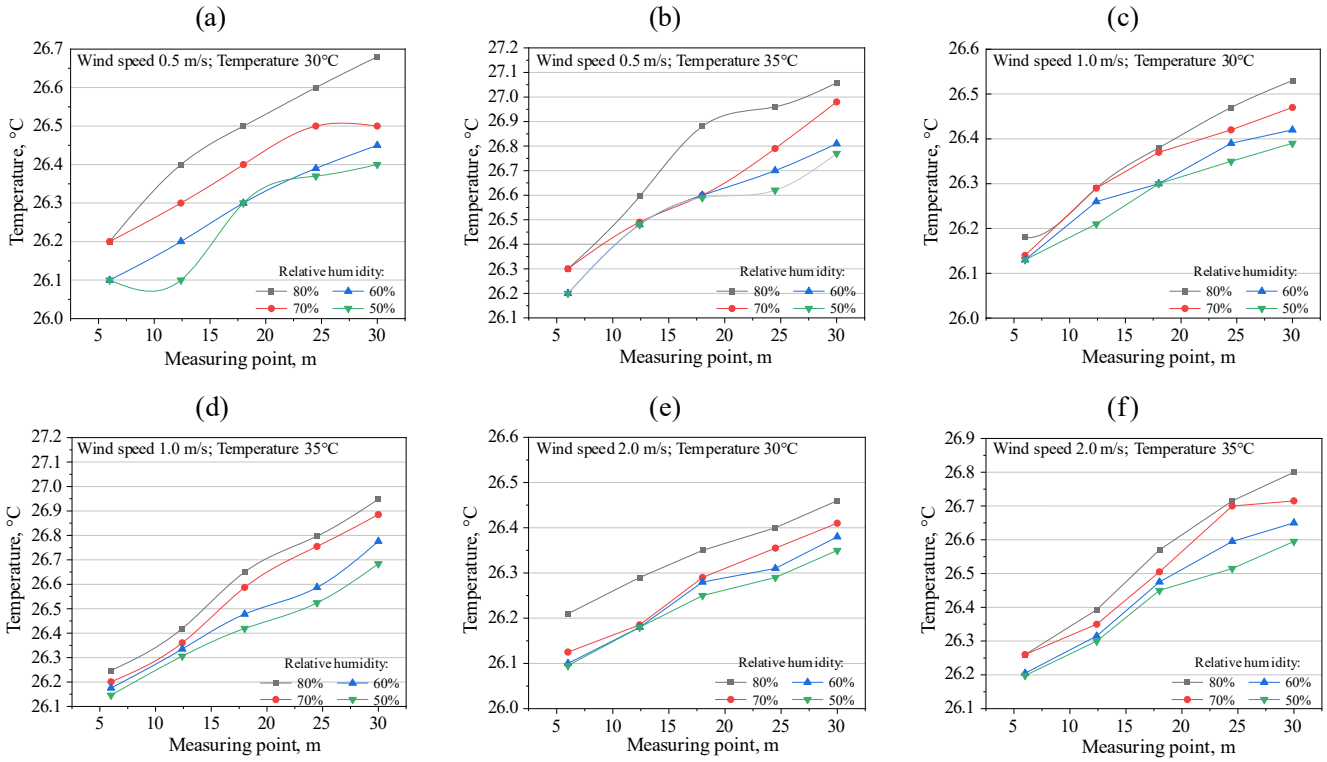

Figure 5. Trend of air flow temperature change with different humidity under six working conditions: (a)-(f) experimental points 1-6

To compare the correlation coefficients, the wind speed is fitted to the first coefficient A, and the temperature is fitted to coefficient B. The fitting equations of the three most suitable influencing factors of wind speed, temperature, humidity, and temperature rise rate are obtained.

Fitting equation between wind speed and the first coefficient:

$$R^2 = 0.9972,\ y = 1.28 - 9.32x + 27.23x^2. \quad (6)$$

Fitting equation between temperature and the second coefficient:

$$R^2 = 0.9847,\ y = 49.18 - 121.71x + 188.99x^2. \quad (7)$$

According to the fitting of the above two equations into the exponential function, the three equations are combined to obtain the fitting equation of wind speed, humidity and temperature to the temperature rise rate:

$$t_1 = (1.28 - 9.32v + 27.23v^2)^{e^{(49.2 - 121.7T + 188.9T^2)}}, \quad (8)$$

where:

t_1 – the rate of temperature rise,°C/m;
v – is the wind speed, m/s;
T – the surrounding rock temperature,°C;
R – the humidity,%,

3.2. Verification of simulation results

The experimental data are compared with numerical simulation results obtained using ANSYS Fluent. The coordinates of the corresponding points are selected in the Cartesian coordinate system based on the position parameters of each measurement point during the experimental measurement. The simulation results for each measurement point are extracted. In this study, wind speeds of 0.5 m/s, temperatures of 35°C, and relative humidities of 60, 70 and 80% are selected for comparison to verify the simulation results. The default temperature scale in the simulation software is the thermodynamic absolute temperature scale. We unified the temperature scale into the Celsius scale to compare the measured data and calculate the relative error. The measured and simulated temperature changes are shown in Figure 6.

Figure 6 shows an error between the simulated and measured temperatures. The maximum absolute error is 0.14°C, the minimum is 0.03°C, and the average value is 0.053°C. The maximum relative error between the simulated and measured temperature is 0.52%, the minimum is 0.07%, and the average is 0.30%. The simulation results indicate that the error at each measurement point does not change significantly relative to the measured temperature. Within the allowable range, the variation curves of the simulated and measured temperatures interweave. The overall trend of the curves is consistent. However, at 60% relative humidity, the measured temperature curve shows a significant discrepancy compared to the simulated curve. The main reasons for this phenomenon are as follows: when the relative humidity is 60%, the water evaporation rate in the simulation increased significantly compared to the actual rate. This led to a relatively large temperature error. In the experiment, because a person holds the temperature-measuring instrument, it will also affect the temperature.

Based on the measured and simulated data, SPSS is used to conduct a significance test of differences in the three primary influences of humidity on temperature mentioned above, as shown in Table 1.

Table 1. Significance analysis of data difference

Relative humidity	*F*	*P*-value	*F* crit
RH = 80%	0.074074	0.798966	6.388233
RH = 70%	0.947368	0.730059	9.473684
RH = 60%	0.023324	0.886013	7.708647

If the *F* value is less than the *F* critical value and the *P*-value is higher than 0.05, this indicates that there is no significant difference between the two groups of data.

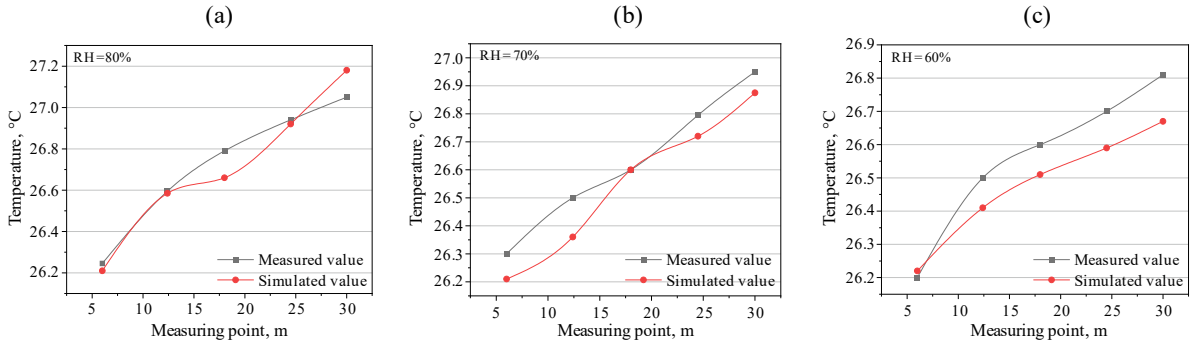

Figure 6. Trend map of measured temperature and simulated temperature

Table 1 shows that there is no significant difference between the simulated and measured data, indicating that the two are relatively close and that the numerical simulation is successful.

The experiments and simulations in this paper mainly focused on the temperature rise of the airflow over a 30-meter length. However, in long-distance ventilation systems, the heat and moisture exchange between the airflow and the surrounding rock is a continuous, dynamic process. Future research will extend the lengths of the simulated and experimental tunnels, examine the pattern of airflow temperature rise rate as the ventilation distance increases, and investigate the dynamic evolution of the rock temperature field over time during ventilation. Provide differentiated technical solutions for the prevention of mine thermal hazards under different geological conditions.

4. Conclusions

Fluent numerical simulation and experimental results show that, with increasing relative humidity in the airflow, the rate of rise in airflow temperature gradually increases. The maximum temperature is 0.038°C/m. As the wind speed increases, the heat exchange time between the airflow and the surrounding rock decreases. The intensity of convective heat transfer is affected, and the airflow temperature increases relatively slowly.

The fitting procedure was performed using the cftool toolbox in MATLAB. The corresponding mathematical relationship describing the temperature rise was obtained. The significance analysis of data differences indicates that the simulated data are in good agreement with the measured data. Therefore, the simulation results demonstrate reliable predictive capability.

Author contributions

Conceptualization: ZS; Data curation: QW; Formal analysis: YL; Funding acquisition: ZS; Investigation: ZS; Methodology: YL; Project administration: ZS; Resources: YL; Software: YL; Supervision: YL; Validation: QW; Visualization: QW; Writing – original draft: ZS; Writing – review & editing: YL. All authors have read and agreed to the published version of the manuscript.

Funding

This research was funded by the Department of Education of Liaoning Province under Grant No. LJ212510153045. This research was funded by the PhD research initiation project of Liaoning province “Fault diagnosis and on-demand regulation of mine ventilation systems based on data-driven flow patterns”.

Acknowledgements

Special thanks are extended to the technical teams at Shenyang Jianzhu University for their valuable assistance with data collection and simulation. Appreciation is also extended to the staff at the experimental mine for their technical assistance and cooperation during the field measurements.

Conflicts of interest

The authors declare no conflict of interest.

Data availability statement

The original contributions presented in the study are included in the article, further inquiries can be directed to the corresponding author.

References

[1] Huang, L., Wei, Y., Chen, Z., Wang, Z., Liu, Y., Sun, L., & Li, C. (2024). Thermal hazard evaluation and prediction in deep excavations for sustainable underground mining. *Sustainability*, *16*(24), 10863. https://doi.org/10.3390/su162410863

[2] Guo, P.Y., Bu, M.H., Zhang, P., & He, M.C. (2022). Research progress on the prevention and utilization of mine geothermal energy. *Chinese Journal of Engineering*, *44*(10), 1632-1651. https://doi.org/10.13374/j.issn2095-9389.2022.04.11.002

[3] You, B., Chen, Y., Yang, M., Gao, K., Cui, D., & Lu, M. (2024). Management of thermal hazards in deep mines in China: Applications and prospects of mine cooling technology. *Water*, *16*(16), 2347.https://doi.org/10.3390/w16162347

[4] Walls, D.B., Banks, D., Boyce, A.J., & Burnside, N.M. (2021). A review of the performance of minewater heating and cooling systems. *Energies*, *14*(19), 6215.https://doi.org/10.3390/en14196215

[5] Wang, X., Wang, Y., Lai, X., Wang, G., & Sang, C. (2025). Investigation of heat stress and thermal response in deep hot-humid underground environments: A field and experimental study. *Building and Environment*, *270*, 112506. https://doi.org/10.1016/j.buildenv.2024.112506

[6] Roy, S., Mishra, D.P., Bhattacharjee, R.M., & Agrawal, H. (2022). Heat stress in underground mines and its control measures: A systematic literature review and retrospective analysis. *Mining, Metallurgy & Exploration*, *39*(2), 357-383. https://doi.org/10.1007/s42461-021-00532-6

[7] Cai, M.F., Ma, M.H., Pan, J.L., Xi, X., & Guo, Q.F. (2022). Co-mining of mineral and geothermal resources: a state-of-the-art review and future perspectives. *Chinese Journal of Engineering*, *44*(10), 1669-1681. https://doi.org/10.13374/j.issn2095-9389.2022.08.24.001

[8] Guo, M., Qin, Y., Wang, D., Wang, S., Tang, F., & Liu, P. (2024). Prediction of airflow temperature in coal mining face under the influence of multiple heat sources coupling: Numerical simulation and verification. *Case Studies in Thermal Engineering*, *61*, 105128. https://doi.org/10.1016/j.csite.2024.105128

[9] Guo, P., Su, Y., Pang, D., Wang, Y., & Guo, Z. (2020). Numerical study on heat transfer between airflow and surrounding rock with two major ventilation models in deep coal mine. *Arabian Journal of Geosciences*, *13*(16), 756.https://doi.org/10.1007/s12517-020-05725-9

[10] Li, A., Yang, C., & Ren, T. (2016). Modeling and parametric studies for convective heat transfer in large, long and rough circular cross-sectional underground tunnels. *Energy and Buildings*, *127*, 259-267. https://doi.org/10.1016/j.enbuild.2016.05.088

[11] Ghoreishi-Madiseh, S.A., Kalantari, H., Kuyuk, A.F., & Sasmito, A.P. (2019). A new model to analyze performance of mine exhaust heat recovery systems with coupled heat exchangers. *Applied Energy*, *256*, 113922. https://doi.org/10.1016/j.apenergy.2019.113922
[12] Bao, L., Wang, J., Wang, J., & Yu, Z. (2017). The heat recovery technologies of mine waste heat sources. *World Journal of Engineering*, *14*(1), 19-26. https://doi.org/10.1108/WJE-11-2016-0125
[13] Li, Z., Xu, Y. U., Li, R., Jia, M., Wang, Q., Chen, Y., & Han, Z. (2021). Impact of the water evaporation on the heat and moisture transfer in a high-temperature underground roadway. *Case Studies in Thermal Engineering*, *28*, 101551. https://doi.org/10.1016/j.csite.2021.101551
[14] Li, Z., Xu, Y., Jia, M., Liu, H., Pan, W., & Deng, Y. (2021). Numerical simulation on heat hazard control by collaborative geothermal exploitation in deep mine. *Journal of Central South University (Science and Technology)*, *52*(3), 671-680. https://doi.org/10.11817/j.issn.1672-7207.2021.03.002
[15] Wang, G., Hao, R., Liu, X., Xu, H., Xie, S., & Hou, Z. (2024). Numerical simulation of airflow temperature field and cooling in high temperature coal seam working face. *Thermal Science and Engineering Progress*, *48*, 102374. https://doi.org/10.1016/j.tsep.2023.102374
[16] Li, Z., Wang, J., Xu, Y., Li, G., Yuan, T., & Zhang, M. (2022). Heat hazard control in excavation engineering: Numerical simulation of heat transfer characteristics of high temperature tunnel with movable thermal insulation layer. *Thermal Science and Engineering Progress*, *34*, 101393. https://doi.org/10.1016/j.tsep.2022.101393
[17] Wang, W., Zhang, C., Yang, W., Xu, H., Li, S., Li, C., Ma, H., & Qi, G. (2019). In situ measurements and CFD numerical simulations of thermal environment in blind headings of underground mines. *Processes*, *7*(5), 313. https://doi.org/10.3390/pr7050313
[18] Jia, T., Ma, H., & Gao, K. (2025). Decision on optimal airflow regulation solution set based on heat and airflow coupling characteristics of mine airflow in time series. *Plos One*, *20*(5), e0320326. https://doi.org/10.1371/journal.pone.0320326
[19] Siyu, Z., Xingdong, Z., Ang, L., & Lei, D. (2025). Study on the change rule of airflow temperature field in ultra-deep mining shaft. *Scientific Reports*, *15*(1), 6999. https://doi.org/10.1038/s41598-025-88247-2
[20] Kang, F., Men, J., Qin, B., Sun, G., Chen, R., Zhang, W., & Ye, Z. (2025). Comparative study on the evolution of airflow temperature and valid ventilation distance under different cooling strategies in high-temperature tunnels for mining thermal energy. *Fire*, *8*(1), 16. https://doi.org/10.3390/fire8010016
[21] Che, J., Li, A., Guo, J., Ma, Y., Li, J., Yang, C., & Che, L. (2024). Theoretical and experimental investigation on the thermal penetration depth in the surrounding rock of a deeply buried high-temperature tunnel. *International Journal of Thermal Sciences*, *198*, 108876. https://doi.org/10.1016/j.ijthermalsci.2023.108876
[22] Abdelrazik, A.S., Osama, A., Allam, A.N., Shboul, B., Sharafeldin, M.A., Elwardany, M., & Masoud, A.M. (2023). ANSYS-Fluent numerical modeling of the solar thermal and hybrid photovoltaic-based solar harvesting systems. *Journal of Thermal Analysis and Calorimetry*, *148*(21), 11373-11424. https://doi.org/10.1007/s10973-023-12509-2
[23] Sarkar, S., & Rawat, B. (2024). Numerical simulation of pseudoplastic fluid flow over a square cylinder using ANSYS Fluent. *International Journal of Fluid Mechanics Research*, *51*(6), 43-52. https://doi.org/10.1615/InterJFluidMechRes.2024053083
[24] Yi, H., Kim, M., Lee, D., & Park, J. (2022). Applications of computational fluid dynamics for mine ventilation in mineral development. *Energies*, *15*(22), 8405. https://doi.org/10.3390/en15228405
[25] Zhang, L., Zhou, G., Ma, Y., Jing, B., Sun, B., Han, F., & Chen, X. (2021). Numerical analysis on spatial distribution for concentration and particle size of particulate pollutants in dust environment at fully mechanized coal mining face. *Powder Technology*, *383*, 143-158. https://doi.org/10.1016/j.powtec.2021.01.039
[26] Kumar, A.R., Salami, O., Amoah, N.A., & Xu, G. (2024). Comparative analysis of different CFD turbulence models for a diesel pool combustion event in an underground mine: A case study. *International Journal of Mining, Reclamation and Environment*, *38*(7), 549-561. https://doi.org/10.1080/17480930.2024.2335708
[27] Lian, B., Qiao, D., Yang, T., Wang, J., Chen, J., Li, S., & Long, G. (2024). Research on pipeline transportation design of tailings slurry from a tin mine in Yunnan Province based on ANSYS-Fluent. *Nonferrous Metals Science and Engineering*, *15*(3), 407-421. https://doi.org/10.13264/j.cnki.ysjskx.2024.03.011

Дослідження впливу закономірностей формування теплового середовища шахти на зміну температури повітряного потоку

Ч. Шень, І. Лі, Ц. Ван

Мета. Метою роботи є дослідження впливу таких чинників як вологість і швидкість руху повітря на зміну температури повітряного потоку в тепловому середовищі шахти.

Методика. Експеримент із тепло- та вологообміну в шахті поєднано з чисельним моделюванням. За допомогою програмного комплексу ANSYS Fluent змодельовано та проаналізовано вплив вологості повітряного потоку на температурне поле за різних температур і швидкостей руху повітря. Аналогічний експеримент проведено в експериментальній шахті з вимірюваннями за різних температурних режимів і швидкостей повітря. Досліджено зміну теплообміну між повітрям і навколишніми породами виробки за різної вологості.

Результати. Результати чисельного моделювання та експериментальних досліджень показали, що зі збільшенням відносної вологості повітряного потоку швидкість підвищення його температури поступово зростає. Максимальне значення становить 0.038°C/м. Збільшення швидкості повітря скорочує час теплообміну, що призводить до зменшення темпу зростання температури. Розроблено емпіричну модель, яка описує взаємозв'язки між швидкістю повітря, температурою, вологістю та швидкістю підвищення температури.

Наукова новизна. У роботі вологість ураховано як ключовий фактор та запропоновано емпіричну модель зміни температури повітряного потоку в умовах підвищеної вологості шахтного середовища.

Практична значимість. Отримані результати створюють наукове підґрунтя для прогнозування та регулювання температури повітря в шахтах із підвищеною температурою, сприяють покращенню теплового комфорту та безпеки праці підземного персоналу, а також можуть бути використані під час проєктування систем вентиляції та розроблення заходів щодо зниження теплової небезпеки.

Ключові слова: *шахта; теплове середовище; ANSYS Fluent; чисельне моделювання; зміна температури; теплообмін*

Publisher's note

All claims expressed in this manuscript are solely those of the authors and do not necessarily represent those of their affiliated organizations, or those of the publisher, the editors and the reviewers.